Korean J. Chem. Eng., **25**(6), 1539-1545 (2008)

Effects of silyl concentration, hydrogen concentration, ion flux, and silyl surface diffusion length on microcrystalline silicon film growth

Shutang Wen*,, Liwei Zhang***, Jingxiao Lu*,†, Yuxiao Li*, and Zhiyong Du***

*School of Chemistry and Chemical Engineering, Xinxiang University, Xinxiang, 453000, China
**School of Physics and Engineering, Zhengzhou University, Zhengzhou, 450052, China
***Physics Department, Xinxiang University, Xinxiang, 453000, China
(*Received 29 January 2008 • accepted 25 March 2008*)

Abstract−Two sets of μc-Si : H films as a function of pressure were fabricated by very-high-frequency plasma enhanced chemical vapor deposition (VHF-PECVD). Deposition rate, Raman crystallinity, and photo/dark conductivity were investigated under both low and high power conditions. A plasma fluid model and a surface hydride-dependent precursor diffusion model were constructed to understand the evolution of microcrystalline silicon under low and high power conditions. Silyl, hydrogen, ion flux, silyl surface diffusion length are believed to have much influence on film growth rate, crystallinity and photo electronic properties. But the interesting point is that under a certain condition one or more of these parameters dominate μc-Si : H growth, while other parameters have weak influence. Short-life radicals are found to be the possible major factor on the deterioration of photo sensitivity of μc-Si : H films.

Key words: Plasma Model, Surface Diffusion Model, Silicon Film, VHF-PECVD

INTRODUCTION

Twenty years ago, the researchers in Jülich institute first introduced VHF power (>13.56 MHz) to deposit silicon films, and about 10 years later, they introduced μc-Si : H as the absorb layer (i-layer) of p-i-n solar cells. Ever since then, VHF-PECVD has been widely used to fabricate μc-Si : H materials and solar cells, combined with high power/high pressure method [1-4].

However, despite the widespread use of VHF-PECVD processes and the fact that deposition of silicon from silane is one of the best studied VHF-PECVD systems, the details of the chemistry occurring during deposition are not yet well understood.

In recent years, a number of silane plasma models have been published [5,6]. Tachibana et al. developed a plasma model where all the particle balance equations are solved interactively assuming steady state [7]. While for the electron kinetics, some assume constant electron reaction rate coefficients, others use a Maxwellian or a Druyvesteyn-like electron energy distribution function to calculate the electron reaction rate coefficients. Here, we use a one-dimensional fluid model composed of the Boltzmann equation coupled with the Poisson equation to calculate the electron energy distribution function and particle densities [8,9].

Not only radical formations in the silane plasma but also radical diffusion and abstraction of hydrogen on the film surface have much influence on film growth and crystallization. Thus, we also construct a surface hydride-dependent precursor diffusion model to include the influence of dominant precursor's physisorption, diffusion and reaction, as well as direct chemisorption and insertion Si-Si bond as a function of silyl flux [10].

EXPERIMENTAL

Two sets of microcrystalline silicon thin films were prepared under various deposition pressures at two fixed values of power density. With the power density at 0.44 W/cm^2, silane concentration was kept at 3%, while at 1.1 W/cm^2, silane concentration was kept at 4%, and other parameters were kept as substrate temperature=220 °C, gas flow=150 sccm and electrode distance=1.5 cm.

Raman crystallinity was characterized by Raman spectroscopy, and dark and photo conductivities were measured by a Keithley 6517 electrometer. Film thickness was measured by spectroscopic ellipsometry.

RESULTS AND DISCUSSION

1. Experimental Results

VHF power combined with high pressure and high power is ben-

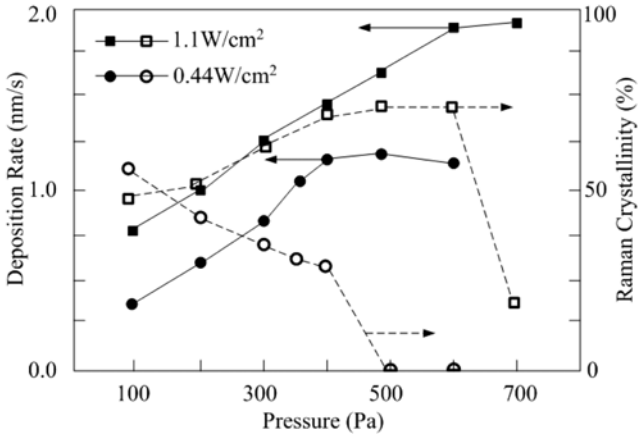

Fig. 1. Deposition rate and Raman crystallinity as a function of pressure with power density fixed at 0.44 W/cm^2 and 1.1 W/cm^2.

†To whom correspondence should be addressed.
E-mail: jxlu2000@163.com

eficial to film growth, and this is mainly ascribed to the low energy and high density of electrons and high atom hydrogen density in the plasma under this condition. In order to study the influence of power density, Fig. 1 gives two sets of data related to two of the most important properties of microcrystalline silicon films at two power densities. The deposition rate increases with increased pressure, except for the lower silane concentration series with pressures more than 350 Pa. Raman crystallinity behaves in a more complicated fashion as a function of pressure with its increasing first and decreasing finally at high power density in contrast to its monotonically decreasing at low power density. Some researchers believed that at low power density atom hydrogen density decreases monotonically with pressure increased by measuring the emission intensities of H_α^* and H_β^* from OES (optical emission spectroscopy) [11]. But our results in Fig. 3(a) show that although atom hydrogen density does not decrease, it increases more slowly than SiH_3 and thus its etching effect is prominently reduced.

While at high power density the atom hydrogen density increases greatly compared with the increase of SiH_3 intensity, so under the dominance of enhanced hydrogen etching, Raman crystallinity increases when pressure is increased. However, the increasing of atom hydrogen density begins to slow down, and growth rate reaches a high value when pressure is further increased, which leads to the reducing of hydrogen etching and silyl surface diffusion length and in turn contributes to the decreasing of Raman crystallinity.

Fig. 2 gives dark and photo conductivity as a function of pressure. As crystallinity increases, both dark and photo conductivity increase, which generally goes well with the fact that when crystal phase increases, both dark and photo conductivity increase. But photo sensitivity does not follow the way in which crystallinity changes. This is probably due to an abrupt enhancement of the density of defects at pressures more than 300 Pa.

2. One-dimensional Fluid Model

In order to understand the experimental phenomena described above, we must first introduce some basic assumptions: 1. Growth rate is determined by silyl flux toward the film surface and its reaction on the surface, which can be calculated via the two models we proposed. 2. Crystallinity is closely related to atom hydrogen, higher silane polymers, ion energy and density, and silyl diffusion length on the film surface.

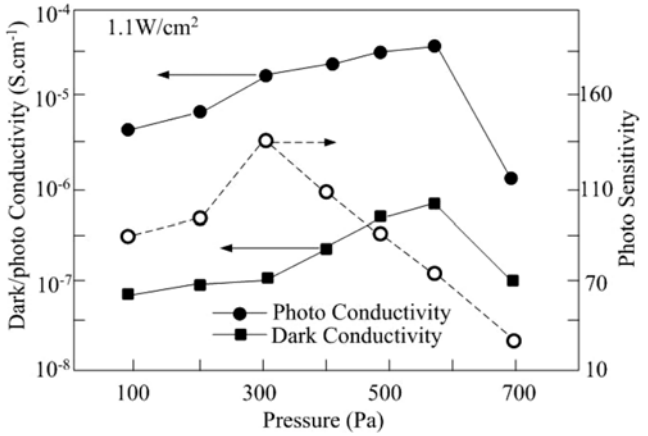

Fig. 2. Dark/photo conductivity and photo sensitivity as a function of pressure.

Self-consistent fluid models have been used to simulate silane plasma [12-15], and the model presented in this article is a self-consistent fluid model. Due to the discharge processes, silane is consumed and hydrogen is dissociated, the composition of the background gas is different form the feedstock gas and is chiefly made of neutrals, ions, and electrons. In fluid models the discharge is described by a combination of balances for the particle, momentum, and energy densities of the ions, electrons, and .neutrals. The electric field is solved self-consistently by using the Poisson equation. The collision rates, the electron transport coefficients, and the average electron energy are obtained by solving the Boltzmann equation for the EEDF.

The species considered in the model for silane are listed as below: The main neutrals are H_2, SiH_4, and Si_3H_8. The main radicals are SiH_3, H, Si_2H_5 and SiH_2. The main ions are $Si_2H_5^+$, SiH_4^+, SiH_3^+. A typical PECVD reactor is not completely filled with the discharge; thus transport of neutrals from the discharge volume to the discharge-free volume and vice versa will occur [16].

In Table 1, the 11 electron-neutral reactions taken into account in the model are presented. These electron-neutral reactions can be divided in three categories: vibrational excitation, dissociation, and ionization reactions. The electron-radical reactions are also considered because it is found that these radical species are abundant at high densities in the discharge In total, seven neutral-neutral reac-

Table 1. Electron impact collisions taken into account in the model

Reaction	Chemical reaction	Ref.
Vibr. exc. 1-3	$SiH_4+e^- \rightarrow SiH_4^{(1\text{-}3)}+e^- \rightarrow SiH_4+e^-$	[17]
Vibr. exc. 2-4	$SiH_4+e^- \rightarrow SiH_4^{(2\text{-}4)}+e^- SiH_4+e^-$	[17]
Ionization	$SiH_4+e^- \rightarrow SiH_2+2H+e^-$	[18]
Ionization	$SiH_4+e^- \rightarrow SiH_2^++2H+2e^-$	[19]
Dissociation	$SiH_4+e^- \rightarrow SiH_3+H+e^-$	[18]
Dissociation	$SiH_4+e^- \rightarrow SiH_3^-+H$	[20]
Dissociation	$Si_2H_6+e^- \rightarrow Si_2H_4^++2H+e^-$	[19]
Dissociation	$Si_2H_6+e^- \rightarrow SiH_3++SiH_2+H+e^-$	[18]
Ionization	$H_2+e^- \rightarrow H_2^++2e^-$	[21]
Dissociation	$H_2+e^- \rightarrow H+H+e^-$	[22]

Table 2. Neutral-neutral reaction incorporated in this model

Chemical reaction	Reaction rate ($cm^{-3}s^{-1}$)	Ref.
$H+SiH_4 \rightarrow SiH_3+H_2$	$2.8\times10^{-11}\exp(-1250/T_{gas})$	[23]
$H+Si_2H_6 \rightarrow Si_2H_5+H_2$	$1.6\times10^{-10}\exp(-1250/T_{gas})$	[23]
$H+Si_2H_6 \rightarrow SiH_3+SiH_4$	$0.8\times10^{-10}\exp(-1250/T_{gas})$	[23]
$H_2+SiH_2 \rightarrow SiH_4$	$3.0\times10^{-12}(1-(1+2.3\times10^{-4}p_0))$	[23]
$SiH_4+SiH_2 \rightarrow Si_2H_6$	$2.0\times10^{-10}(1-(1+0.0032p_0)^{-1})$	[23]
$SiH_3+SiH_3 \rightarrow SiH_4+SiH_2$	1.5×10^{-10}	[23]

Table 3. Ion-ion reaction incorporated in this model

Ion-ion reaction	Reaction rate ($cm^{-3}s^{-1}$)	Ref.
$SiH_3^-+SiH_2^+ \rightarrow SiH_3+SiH_2$	1.2×10^{-7}	[24]
$SiH_3^-+Si_2H_4^+ \rightarrow SiH_3+2SiH_2$	1.0×10^{-10}	[24]
$SiH_3^-+H_2^+ \rightarrow SiH_3+H_2$	0.8×10^{-10}	[24]

tions (Table 2) and three ion-ion reactions (Table 3) are included in the model.

A one-dimensional model for silane VHF plasma consisting of neutrals, radicals, ions, and electrons is presented. The equations solved are the particle balances, assuming a drift-diffusion approximation for the fluxes, and the electron energy balance equation. The self-consistent electric field is obtained from the simultaneous solution of Poisson's equation. The electron-neutral collision rates are expressed as a function of the average electron energy.

$$\frac{\partial n_j}{\partial t} + \frac{\partial \Gamma_j}{\partial z} = S_{rec,j} + S_{flow,j} + S_{pump,j} + S^{rd}_{flow,j} \tag{1}$$

$$\Gamma_j = \mu_j n_j E - D_j \frac{\partial n_j}{\partial z} \tag{2}$$

$$\frac{\partial^2 V}{\partial z^2} = -\frac{e}{\varepsilon_0}\left(\sum_{i=ions} q_i n_i - n_e\right);\ E = -\frac{\partial V}{\partial z} \tag{3}$$

$$\frac{\partial w_e}{\partial t} + \frac{\partial q_w}{\partial x} = -e\Gamma_e E + S_w \tag{4}$$

$$q_w = -\frac{5}{3}\mu_e w_e E = -\frac{5}{3} D_e \frac{\partial W_e}{\partial x} \tag{5}$$

$$V(z=L, t) = V_{VHF}\sin(2\pi\nu_{VHF} t) \tag{6}$$

$$p_{dis.} = \frac{e\pi R^2_{elec}}{\tau} \sum_{\substack{i=charged \\ particles}} \int_0^{\tau}\int_0^{L} E(z,t)\,dz\,dt \tag{7}$$

$$\frac{\partial f}{\partial t} + \nabla_r \cdot (\mathbf{V} f) - \nabla_v \cdot \left(\frac{e}{m_e}\mathbf{E}(\mathbf{r},t) f\right) = \left(\frac{\partial f}{\partial t}\right)_{coll.} \tag{8}$$

Eq. (1) describes particle balances in this model, where n_j is the density and Γ_j is the flux of particle j. The source term $S_{reac,j}$ represents the creation or destruction of corresponding particles j by electron impact collisions with neutrals or by chemical reactions; the flow source term $S_{flow,j}$ and the pump source term $S_{pump,j}$ are introduced to model the inlet of the feedstock gases and the pumping in the deposition reactor, respectively.

$$S_{pump,j} = -\frac{n_j}{\tau} \tag{9}$$

where τ is the average residence time of all neutrals.

$$S^{rd}_{mix,j} = (S_{pump,j} + S_{flow,j})\frac{(V_{reactor} - V_{disch.})}{V_{disch.}} \tag{10}$$

Where the mixing source term $S_{mix,j}$ is introduced to correct the exclusion of radical transport. $V_{reactor}$ is the total volume of the plasma reactor and $V_{disch.}$ is the volume of the discharge.

Eq. (2) describes the drift-diffusion approximation. where μ_j and D_j are the mobility and diffusion transport coefficients, respectively.

Eq. (3) describes the electric field E and potential V.

Eq. (4) describes the electron energy balances. In which q_w is the electron energy density flux and is given by Eq. (5).

Eqs. (6) and (7) give the boundary conditions. EEDF in Eq. (8) is denoted as f(**r**, **v**, t) that specifies the number of electrons at position **r**, with velocity **v** at time t. For further description, see Ref. [9].

By solving these equations, we obtain the simulation results presented below:

Fig. 3 gives the densities of various particles in the plasma calculated based on a one-dimensional fluid model. From Fig. 3(a) and (b), we can see the two most potential candidates to contribute to film growth are SiH_3 and Si_2H_5. Since Si_2H_5 is one order low than SiH_3, and its flux density to the film surface is even lower than SiH_3 flux, the growth rate is mainly determined by the density of SiH_3

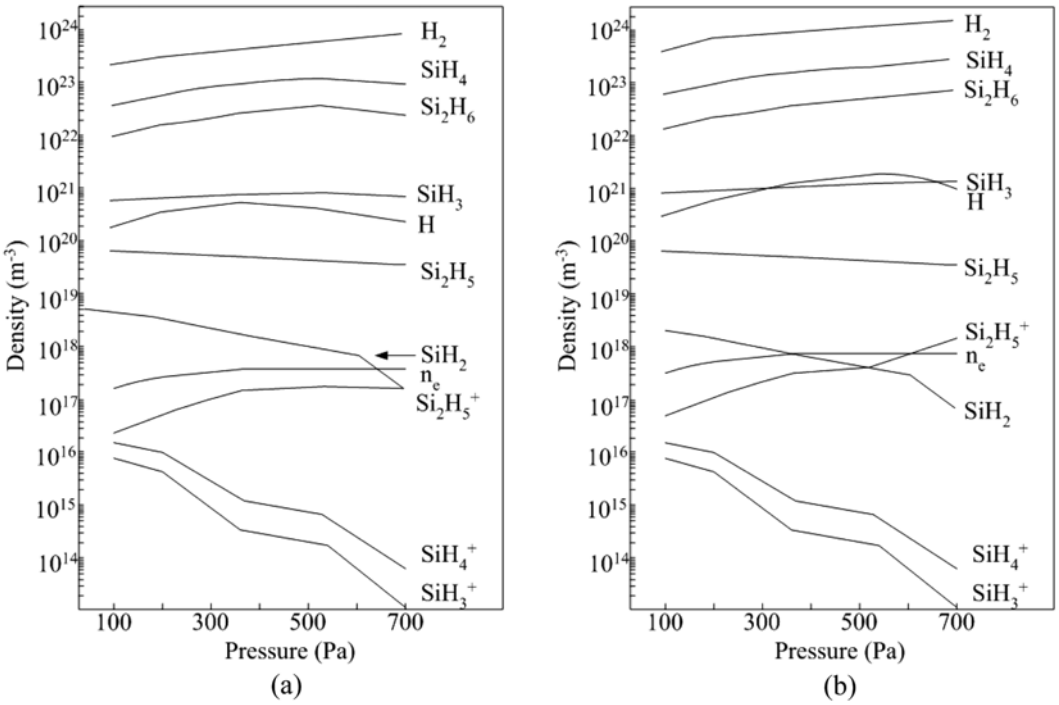

Fig. 3. Densities of neutrals, radicals and ions calculated based on the one-dimensional fluid model at power density of (a) 0.44 W/cm^2 (b) 1.1 W/cm^2.

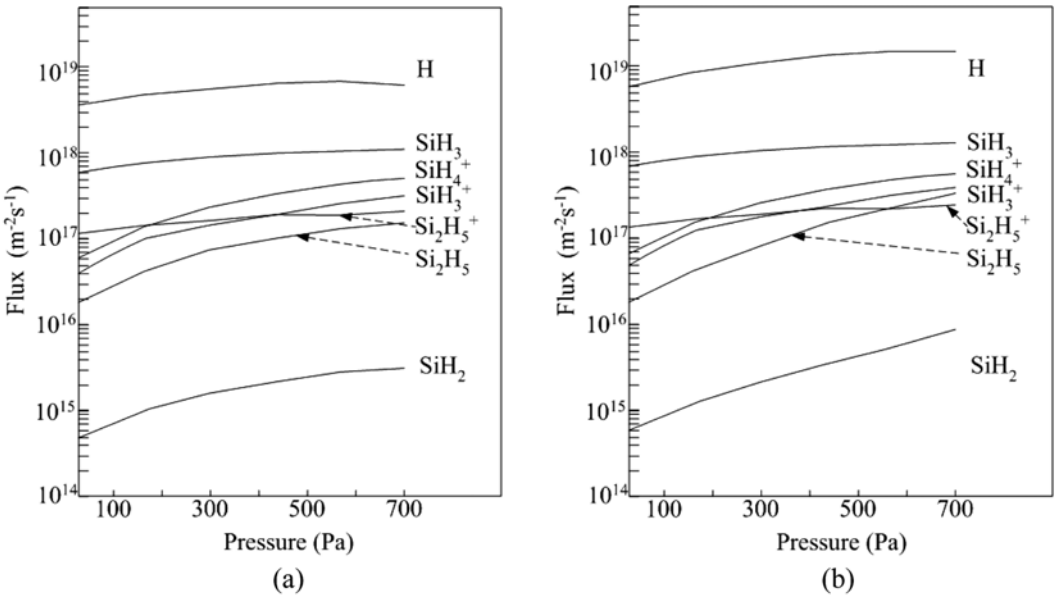

Fig. 4. Flux of neutrals, radicals and ions calculated based on the one-dimensional fluid model at power density of (a) 0.44 W/cm^2 (b) 1.1 W/cm^2.

in the plasma. As we have assumed that radical and ion densities in the plasma might not be the deciding factor, we further give the different flux densities as a function of pressure under low and high power conditions.

Comparing Fig. 4 with Fig. 3, we can see a major difference in that the atom hydrogen flux is much larger than SiH_3 flux, although it's not the case when evaluating density in the plasma. That is why we consider fluxes to the surface rather than densities in the plasma. For both power densities, SiH_3 flux increases with pressure, which explains growth rate with pressure enhanced in Fig. 1. For both power densities, atom hydrogen flux increases prominently when pressure is increased from under 100 Pa; one difference is noted that the flux increasing tendency begins to slow down after 400 Pa for the lower power density, 600 Pa for the higher power density. Positive ion densities increase rapidly with pressure increasing. Another major difference is for the higher power density, the fluxes of Si_2H_5, SiH_2 climb up almost in proportion to pressure.

3. Surface Hydride-dependent Precursor Diffusion Model

Not only electron silane collisions and vapor phase reactions of radicals, neutrals, and ions in the plasma determine silicon film growth, but also radical reactions on the film surface are very important for film growth rate and crystallinity. According to the surface diffusion model, the diffusion length of radicals on the surface determines film crystallinity and other properties [25-28]. Those short life-time radicals, like SiH_2, Si_2H_5, are too reactive to have substantial time to diffuse on the surface; their incorporation leads to an undesirable anisotropic columnar growth. Here we consider another often neglected factor, the diffusion length of SiH_3. We obtained its

Table 4. List of reactions of SiH_3 and H used in this model

No	Reaction	Description	Rate
A	$\equiv Si\text{-} + SiH_{3(g)} \rightarrow \equiv Si\text{-}SiH_3$	Addition of SiH_3 to db	$S_0 \cdot \varphi_{Si} \cdot \theta_0$
B	$\equiv(SiH_x) + SiH_{3(g)} \rightarrow \equiv(SiH_x)SiH_3$	Physisorption of SiH_3	$S_1 \cdot \varphi_{Si} \cdot \theta_x$
C	$\equiv(SiH_x)SiH_3 + SiH_{3(g)} \rightarrow \equiv(SiH_x) + Si_2H_6$	Abstraction of physisorbed SiH_3 by SiH_3	$S_2 \cdot \varphi_{Si} \cdot \theta_4$
D	$\equiv(SiH_x)SiH_3 + H_{(g)} \rightarrow \equiv(SiH_x) + SiH_4$	Abstraction of physisorbed SiH_3 by H	$S_2' \cdot \varphi_H \cdot \theta_4$
E	$\equiv(SiH_x) + SiH_{3(g)} \rightarrow \equiv(SiH_{x-1}) + SiH_{4(g)}$	Abstraction of H by SiH_3	$V_{a1} \cdot \varphi_{Si} \cdot \theta_x$
F	$\equiv(SiH_x)SiH_3 \rightarrow \equiv(SiH_x) + SiH_{3(g)}$	Desorption of physisorbed SiH_3	$V_{d1} \cdot \theta_4$
G	$\equiv(SiH_x)SiH_3 \rightarrow \equiv(SiH_{x-1}) + SiH_{4(g)}$	Abstraction of H by physisorbed SiH_3	$V_{a3} \cdot \theta_4 \cdot \theta_x$
H	$\equiv(SiH_x)SiH_3 + \equiv Si\text{-} \rightarrow \equiv Si\text{-}H_x + \equiv SiSiH$	Chemisorption of physisorbed SiH_3	$V_{hx} \cdot \theta_4 \cdot \theta_0$
I	$\equiv(SiH_x)SiH_3 + \equiv SiH_y \rightarrow \equiv SiH_x + \equiv(SiH_y)SiH_3$	Hopping of physisorbed SiH_3 on hydrides	$V_{hx} \cdot \theta_4 \cdot \theta_1$
J	$2\equiv(SiH_x)SiH_3 \rightarrow 2\equiv SiH_x + Si_2H_{6(g)}$	Desorption of two physisorbed SiH_3	$V_{d2} \cdot \theta_4 \cdot \theta_4$
K	$\equiv(SiH_x) + \equiv(SiH_y) \rightarrow \equiv(SiH_{x-1})\text{-}(SiH_{y-1}) + H_{2(g)}$	Formation of Si-Si bond by recombination of 2 hydrides	$V_{pxy} \cdot \theta_x \cdot \theta_y$
L	$\equiv Si\text{-}Si\equiv + SiH_{3(g)} \rightarrow \equiv SiSiH_3 + \equiv Si\text{-}$	SiH_3 insertion into Si-Si	$V_{i1} \cdot \varphi_{Si} \cdot f \cdot \theta_5$
M	$H_xSi\text{-}Si\equiv + H_{(g)} \rightarrow H_{x+1}Si + \equiv Si\text{-}$	H insertion into Si-Si	$V_{i1}' \cdot \varphi_H \cdot f \cdot \theta_5$
N	$\equiv Si\text{-}Si\equiv + H_3Si(SiH_x)\equiv \rightarrow 2\equiv SiSiH_x + \equiv Si\text{-}$	Insertion of physisorbed SiH_3 into Si-Si	$V_{i3} \cdot \theta_4 \cdot f \cdot \theta_5$
O	$\equiv(SiH_x) + \equiv(SiH_y) \rightarrow 2\equiv(SiH_y) + H_{2(g)}$	Recombination of 2 hydrides forming dangling bonds	$V_{r1} \cdot \theta_x \cdot \theta_y$

variant diffusion length on the surface based on the quantitative kinetic model [10]. This model involves a set of valence, site, reaction balance equations; we added hydrogen flux into the model while the original model only contains SiH_3 flux. Under high growth rate, physisorbed SiH_3 diffusion dominates film growth according to the experiments monitoring the surface topology evolution using atomic force microscopy [29]. Gallagher et al. [30], Perrin et al. [31], Ganguly et al. [32], Matsda et al. [26], have proposed growth models based on dominant surface diffusion of physisorbed precursors. The surface diffusion growth models involve physisorption of the growth precursors, which may then diffuse around on the surface and get chemisorbed upon reaching a dangling bond site on the surface or may abstract hydrogen atoms before reaching dangling bonds creating new dangling bonds onto which other precursor radicals may chemisorb. Since these models only consist of a few reaction mechanisms, they present rather simple pictures of the formation of silicon films. In the following model, altogether 15 reactions (See Table 4) are proposed as dominant growth pathways.

These reactions may be divided into two categories. One occurs directly between the incident radicals and surface bonds/sites (through Eley-Rideal mechanism, E-R); the other occurs between different species on the surface (through Langmuir-Hinshelwood mechanism). The first kind of reaction is quantified as the product of 1) a reaction probability; 2) the radical flux of SiH_3 or H φ_{Si}/φ_H; and 3) the fraction surface coverage of the species, θ_x (x=0, 1, 2, 3, 4, 5). The second kind of reaction is quantified as the product of 1) the reaction rate constant, V_n; and 2) the product of the fractional surface coverage of the relevant species θ_x and θ_y (x, y=0, 1, 2, 3, 4, 5). In Table 4, these reactions are specified as follows: The incident radicals directly react with surface bonds/sites (Reactions A-D). Silyl radicals may chemisorb on the dangling bonds (Reaction A). S_0 is taken as 0.25 corresponding to the approximate fraction surface area of a dangling bond on a SiH_3 radical; Silyl radicals may also physisorb on the surface (Reaction B). S_1 is also set to 0.25, neglecting the detailed bond configuration of physisorbed SiH_3 on the surface. Silyl radicals may impinge on the physisorbed SiH_3 and abstract them (Reaction C). S_2 is set to 0.25×0.4=0.1, because the dangling bond of an incident silyl must point to and attack from the sides of a physisorbed SiH_3; whereas the incident H may also impinge on the physisorbed SiH_3 and abstract it. We assume that this reaction has no kinetic barrier, and S_2' is set to 0.4, since H must also attack from the sides of a physisorbed SiH_3. Silyl radical may also directly abstract a surface H, thus creating a dangling bond on the surface. The reaction probability V_{a1} is also set to 0.25. Once the silyl radical becomes physisorbed on the surface, there are several possible surface reactions that may occur. It can simply desorb from the surface (Reaction F), or abstract a neighboring hydride (Reaction G). It can also hop onto a dangling bond (Reaction H), or from one hydride to another (Reaction I). Two neighboring physisorbed radicals may recombine and desorb (Reaction J). Two neighboring hydrides may recombine to form surface Si-Si bonds (Reaction K). These recombination reactions may occur between tri-hydride and tri-hydride (E_{p33}), tri-hydride and di-hydride (E_{p33}), tri-hydride and mono-hydride (E_{p31}), di-hydride and di-hydride (E_{p22}), di-hydride and mono-hydride (E_{p21}), mono-hydride and mono-hydride (E_{p11}). During film growth, there is a distribution of weak and strong Si-SI bonds that are different in bond length and angles. The impinging and diffusing radicals may insert into the weak Si-Si bonds (Reactions K-N), but a constant fraction is assumed (f=0.1). Reaction O denotes the recombination of two hydrides to form two dangling bonds if the two Si atoms onto which they bind are too far from each other. φ_{Si} and φ_H are the SiH_3 and H flux. A list of reaction rate parameters used in the model is presented in the Table 5.

Assume that there are N Si atoms on the surface with 4N bonds. The 4 N bonds are made of N_0 dangling bonds, N_h Si-H bonds, N_s surface Si-Si bonds and N_b bulk Si-Si bonds. And suppose one dangling bond or one physisorbed SiH_3 dominates the energetics and kinetics of that surface Si atom. The valence balance is written as:

$$0.75\theta_0+\theta_h+2\theta_5+0.75\theta_4=0.75 \tag{11}$$

Where θ_0 (N_0/N) and θ_4 (N_4/N) are the fractional site coverage for dangling bonds and physisorbed radicals, respectively; θ_h (N_h/4 N) and θ_5 (N_5/4 N) are surface Si-Si and Si-H bond fraction respectively.

$$\theta_0+\theta_1+\theta_2+\theta_3+\theta_4=1 \tag{12}$$

Where θ_1, θ_2, θ_3 are the mono-, di- and tri-hydride fractional site densities, added by θ_0, θ_4 equals unity. The relation of θ_1, θ_2, θ_3 and θ_h is given by Eq. (12)

Table 5. List of reaction rate parameters in the model. Note that $V_n=A_n\exp(-E_n/K_BT)$, k_B is Boltzmann's constant, and h is Planck's constant. E_n is obtained from Refs. [10, 33-37]

Reaction	Parameter values				Reaction	Parameter values			
A		S_0		0.25	J	A_{d2}	k_BT/h	E_{d2}	0.7 eV
B		S_1		0.25	K_{11}	A_{p11}	$10^{-10}k_BT/h$	E_{p11}	0.6 eV
C		S_2		0.10	K_{12}	A_{p12}	$10^{-10}k_BT/h$	E_{p12}	0.45 eV
D		S_2'		0.25	K_{13}	A_{p13}	$10^{-10}k_BT/h$	E_{p13}	0.35 eV
E	A_{a1}	0.25	E_{a1}	0.4 eV	K_{22}	A_{p22}	$10^{-10}k_BT/h$	E_{p22}	0.3 eV
F	A_{d1}	k_BT/h	E_{d1}	0.7 eV	K_{23}	A_{p23}	$10^{-10}k_BT/h$	E_{p23}	0.25 eV
G	A_{a3}	$0.1k_BT/h$	E_{a3}	0.4 eV	K_{33}	A_{p33}	$10^{-10}k_BT/h$	E_{p33}	0.2 eV
H	A_h	k_BT/h	E_h	0.3 eV	L	A_{i1}	0.25	E_{i1}	0.5 eV
I_1	A_{h1}	k_BT/h	E_{h1}	0.2 eV	M	A_{i1}'	1	E_{i1}'	0.5 eV
I_2	A_{h2}	k_BT/h	E_{h2}	0.3 eV	N	A_{i3}	k_BT/h	E_{i3}	0.7 eV
I_3	A_{h3}	k_BT/h	E_{h3}	0.3 eV	O	A_{r1}	k_BT/h	E_{r1}	1.9 eV

$$0.25\theta_1+0.5\theta_2+0.75\theta_3=\theta_h \quad (13)$$

$$V_{a1}\varphi_{Si}\theta_{HT}+V_{a3}\theta_4\theta_{HT}+(V_{i1}\varphi_{Si}+V_{i3}\theta_4)f\theta_5+2V_{r1}\theta_{HT}\theta_{HT}-S_0\varphi_{Si}\theta_0 - V_h\theta_4\theta_0+V'_{i1}\varphi_H f\theta_5-S'_2\varphi_H\theta_4=0 \quad (14)$$

$$S_1\varphi_{Si}\theta_{HT}-S_2\varphi_{Si}\theta_4-V_{a3}\theta_4\theta_{HT}-V_{d1}\theta_4-2V_{d2}\theta_4\theta_4-V_{i3}\theta_4 f\theta_5 - V_{heff}\theta_0\theta_4+V'_{i1}\varphi_H f\theta_3\theta_5=0 \quad (15)$$

$$S_2\phi_{Si}\theta_4\frac{\theta_1}{\theta_{HT}}-S_1\phi_{Si}\theta_1-V_{a1}\phi_{Si}\theta_1-V_{a3}\theta_4\theta_1+V_{d1}\theta_4\frac{\theta_1}{\theta_{HT}}+V_{p23}\theta_2\theta_3 + 2V_{p22}\theta_2\theta_2-V_{p13}\theta_1\theta_3-V_{p13}\theta_1\theta_3-2V_{p11}\theta_1\theta_1 - V_{r1}\theta_1\theta_{HT}+V_h\theta_0\theta_4\frac{\theta_1}{\theta_{HT}}+V'_{i1}\varphi_H f\theta_1\theta_5=0 \quad (16)$$

$$S_2\varphi_{Si}\theta_4\frac{\theta_2}{\theta_{HT}}-S_1\varphi_{Si}\theta_2-V_{a1}\varphi_{Si}\theta_2-V_{a1}\varphi_{Si}\theta_2+V_{d1}\theta_4\frac{\theta_2}{\theta_{HT}}+2V_{p33}\theta_3\theta_3 + 2V_{p22}\theta_2\theta_2+V_{p13}\theta_1\theta_3-V_{p12}\theta_1\theta_2-V_{r1}\theta_3\theta_{HT} + V_h\theta_0\theta_4\frac{\theta_2}{\theta_{HT}}+V'_{i1}\varphi_H f\theta_2\theta_5=0 \quad (17)$$

Eqs. (14)-(17) give the balances for dangling bonds, physisorbed radicals, mono-hydride and di-hydride. By numerical computation we obtain the growth rate R_G and diffusion length L_D on the surface as defined in Ref. [10].

$$R_G=a\cdot(S_0\varphi_{Si}\theta_0+V_{i1}\varphi_{Si}f\theta_5+V_h\theta_0\theta_4+V_{13}\theta_4 f\theta_5) \quad (18)$$

$$L_D=d\sqrt{\frac{(V_{h1}\theta_1+V_{h2}\theta_2+V_{h3}\theta_3)\theta_1}{V_{a3}\theta_{HT}+V_d+V_h\theta_0+V_{d2}\theta_4+V_{13}f\theta_5+S_2\varphi_{Si}}} \quad (19)$$

Where a is the Si-Si bond length (~2.4 Å) and d is the average distance per hop, and is set to 0.37 nm.

By taking silyl and hydrogen flux that was calculated in the previous plasma model into consideration, we've obtained growth rate increasing with pressure, which generally goes well with the experimental results (See Fig. 5(a)). When silyl flux is increased, its diffusion length decreases fast, which is detrimental to crystallization. From Fig. 5(b), we see SiH_3 diffusion length decreases rapidly with silane flux flowing to the surface. Since dangling bonds remain almost unchanged and only make up a small fraction compared with hydrides coverage, the cause of diffusion length decrease is not because of dangling bonds which may bind with SiH_3, and thus reduce diffusion length. With the increasing of SiH_3 flux flowing to the surface, tri-hydrides coverage of the surface increases greatly and that is the main cause of a deterioration of diffusion length. This may be an important reason for film crystallinity deterioration under high growth rate deposition.

Now we will apply our assumption to explain microcrystalline silicon growth. As we can see from Figs. 1, 2 and 4(a), our simulation results show growth rate is mainly determined by silyl (SiH_3) flux and hydrogen flux reaching the surface, not by their densities in the plasma. Both from Figs. 4(a) and (b), we see the fluxes of short life radicals and ions are more than one order lower than that of SiH_3. Only under high pressure the fluxes of ions are close to that of SiH_3 and the ions contribution to film growth cannot be neglected [38,39]. We claimed the flux of silyl and atom hydrogen is directly related with the growth rate of the silicon films. Since the densities of silyl and atom hydrogen are different compared with their fluxes, we believe the fluxes reaching the film surface are more important than their densities in the plasma. Both the fluxes of silyl and atom hydrogen determine the film growth, for at different ratio of silyl flux to hydrogen flux, growth rate varies greatly. This is because of the etching effect of atom hydrogen or its reaction with weak Si-Si bonds and physisorbed SiH3 in our model. But notably, the changing tendency of SiH_3 density is similar to growth rate, of which is believed that the increasing of the densities in the plasma is the reason for the increase of film growth rate. The major difficulty of that belief occurs when applying it to explain the changing tendency of film crystallinity, that is the density of atom hydrogen is rather low and it does not follow the way in which crystallinity changes. For both power densities, from a low pressure atomic hydrogen increases abruptly both its density and flux; then positive ion densities and their corresponding energies show a great enhancement, which eliminates the hydrogen etching effect and becomes to be a dominant factor for crystallization. Finally, when growth rate is high enough, the growing film surface is covered by Si-3H instead of Si-H at low growth rate; silyl diffusion length is very low, film crystallization is finally dominated by the low silyl surface diffusion length so that a microcrystalline film is impossible to be obtained under very high growth rate.

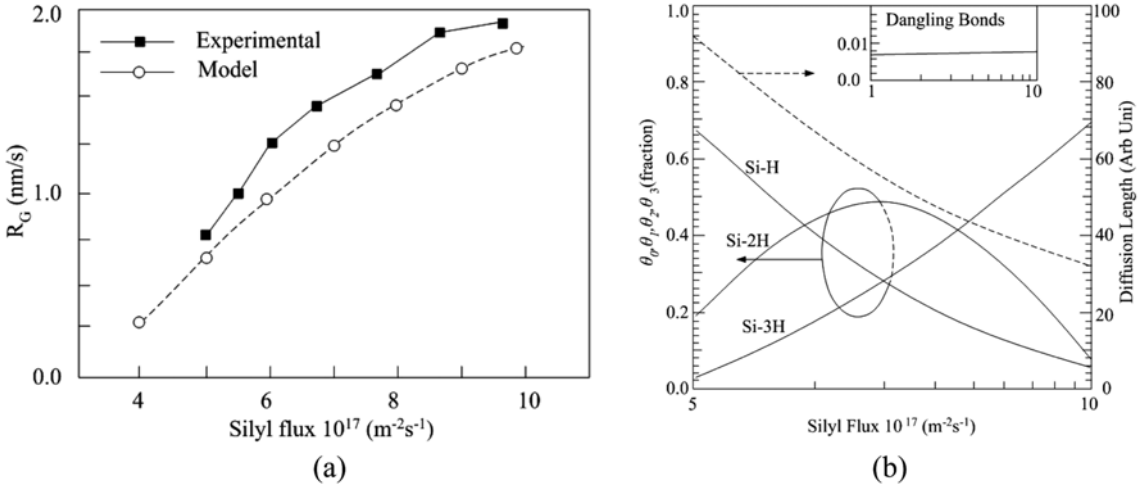

Fig. 5. (a) Growth rate as a function of silyl flux for power density at 1.1 W/cm², (b) Silyl diffusion length as a function of silane flux to film surface calculated based on quantitative kinetic surface reaction model.

In Fig. 2, photo sensitivity decreases although crystallinity increases. In Fig. 4(b), Si_2H_5 and SiH_2 densities undergo a continuous fast growth with pressure increased compared with Fig. 4(a). We think these short life-time radicals incorporated in the film give rise to an enhancement of defects, probably in the grain boundaries.

CONCLUSION

We have investigated microcrystalline silicon thin films deposited under a low power and a high power condition experimentally. To better understand the complex results related to growth rate and Raman crystallinity, we carried out simulations both of plasma kinetics and surface reaction quantitative kinetics. Growth rate enhancement is understood through simulation results, which is mainly due to a balance between SiH_3 and hydrogen flux. One or more factors of the flux of ions, H, and silyl diffusion length dominate the influence on film crystallinity under different conditions. When growth rate is high, diffusion length might ultimately dominate film crystallinity, which was often neglected in previous models and analysis. Short life-time radicals may be detrimental to film crystallinity and photo electronic properties.

ACKNOWLEDGMENTS

This work is supported by the National Key Basic Research and Development Program of China (2006CB202601).

REFERENCES

1. A. Matsuda, M. Takai, T. Nishimoto and M. Kondo, *Sol. Energy Mater. Sol. Cells*, **78**, 3 (2003).
2. M. Takai, T. Nishimoto, M. Kondo and A. Matsuda, *Appl. Phys. Lett.*, **77**, 2828 (2000).
3. S. K. Kim, E. C. Stassinos and H. H. Lee, *Korean J. Chem. Eng.*, **11**, 67 (1994).
4. D. H. Kim, I.-J. Lee, S. W. Rhee and S. H. Moon, *Korean J. Chem. Eng.*, **12**, 572 (1995).
5. K. Bera, B. Farouk and Y. H. Lee, *J. Electrochem. Soc.*, **146**, 3264 (1999).
6. D. J. Dagel, C. M. Mallouris and J. R. Doyle, *J. Appl. Phys.*, **79**, 8735 (1996).
7. K. Tachibana, M. Nishida, H. Harima and Y. Urano, *J. Phys. D: Appl. Phys.*, **17**, 1727 (1984).
8. D. Herrebout, A. Bogaerts, M. Yan, R. Gijbels, et al., *J. Appl. Phys.*, **90**, 570 (2001).
9. D. Herrebout, A. Bogaerts, R. Gijbels, et al., *IEEE Trans. Plasma Sci.*, **31**, 659 (2003).
10. A. Gupta, *Doctor Thesis*, 11, (2001).
11. H. Yong, C. Wu, J. Huang, et al., *Thin Solid Film*, **472**, 125 (2005).
12. Y. B. Hahn and S. J. Pearton, *Korean J. Chem. Eng.*, **17**, 304 (2000).
13. C. A. Faúndez, L. E. Tamblay and J. O. Valderrama, *Korean J. Chem. Eng.*, **21**, 1199 (2004).
14. D. J. Kim, P. J. Lyoo and K. S. Kim, *Korean J. Chem. Eng.*, **20**, 392 (2003).
15. D. J. Kim, J. Y. Kang, A. Nasonova, K. S. Kim and S. J. Choi, *Korean J. Chem. Eng.*, **24**, 154 (2007).
16. G. J. Nienhuis, W. J. Goedheer, E. A. G. Hamers, et al., *J. Appl. Phys.*, **82**, 2060 (1997).
17. M. Kurachi and Y. Nakamura, *J. Phys. D*, **22**, 107 (1989).
18. J. Perrin, J. P. M. Schmitt, G. De Rosny, et al., *Chem. Phys.*, **73**, 383 (1982).
19. E. Krishnakumar and S. K. Srivastava, *Contrib. Plasma Phys.*, **35**, 395 (1995).
20. P. Haaland, *J. Chem. Phys.*, **93**, 4066 (1990).
21. H. Tawara and T. Kato, *At. Data Nucl. Data Tables*, **36**, 167 (1987).
22. A. G. Engelhardt and A. V. Phelps, *Phys. Rev.*, **131**, 2115 (1963).
23. J. Perrin, O. Leroy and M. C. Bordage, *Contrib. Plasma Phys.*, **36**, 3 (1996).
24. A. P. Hickman, *J. Chem. Phys.*, **70**, 4872 (1979).
25. G. Ganguly and A. Matsuda, *Phys. Rev. B*, **47**, 3661 (1993).
26. A. Matsuda, *Thin Solid Films*, **337**, 1 (1999).
27. J. L. Guizot, K. Nomoto and A. Matsuda, *Surface Science*, **244**, 22 (1991).
28. K. Maeda, A. Kuroe and I. Umezu, *Phys. Rev. B*, **51**, 10635 (1995).
29. J. E. Gerbi and J. R. Abelson, *J. Appl. Phys.*, **89**, 1463 (2001).
30. A. Gallagher, *J. Appl. Phys.*, **60**, 1369 (1986).
31. J. Perrin, *J. Non-cryst. Solids*, **137**, 639 (1991).
32. G. Ganguly and A. Matsuda, *J. Non-cryst. Solids*, **166**, 31 (1993).
33. K. R. Bray and G. N. Parsons, *Phys. Rev. B*, **65**, 035311 (2001).
34. A. Gupta and G. N. Parsons, *J. Vac. Sci. Technol. B*, **18**, 1764 (2000).
35. J. Robertson, *J. Appl. Phys.*, **87**, 2608 (2000).
36. W. M. M. Kessels, A. H. M. Smets, D. C. Marra, et al., *Thin Solid Films*, **383**, 154 (2001).
37. D. J. Doren, *Advances in chemical physics*, John Wiley & Sons Inc, New York (1996).
38. M. Heintze, R. Zedlitz and G. H. Bauer, *J. Phys. D: Appl. Phys.*, **26**, 1781 (1993).
39. M. Heintze and R. Zedlitz, *J. of Non-cryst. Solids*, **198-200**, 1038 (1996).